 MCB, vol.5, no.1, pp.37-47, 2008

Micro-CT Based Analysis of a New Paradigm for Vulnerable Plaque Rupture: Cellular Microcalcifications in Fibrous Caps

Yuliya Vengrenyuk*, Luis Cardoso* and Sheldon Weinbaum*,†

Abstract: In this paper, we further investigate the new paradigm for the rupture of thin cap fibroatheroma (TCFA) proposed in Vengrenyuk *et al*. (2006 PNAS 103:14678) using a multilevel micro-CT based 3D numerical modeling. The new paradigm proposes that the rupture of TCFA is due to stress-induced interfacial debonding of cellular - level, 10 – 20 μm microcalcifications in the fibrous cap proper. Such microcalcifications, which lie below the visibility of current *in vivo* imaging techniques, were detected for the first time using confocal microscopy and high resolution microcomputed tomography (micro-CT) imaging in Vengrenyuk *et al*. (2006) In the present study, we use high resolution (7 μm) micro-CT imaging to construct accurate geometries of both these microcalcifications and larger mm size macrocalcifications at the cap shoulders to evaluate their biomechanical stability. The analysis shows that cellular-level calcifications by themselves are not dangerous unless they lie in a region of high background stress. This high level of background stress only occurs in caps whose thickness is < approximately 80 μm. Whereas a spherical microcalcification will increase peak circumferential stress (PCS) by a factor of two, in agreement with previous local analytical solutions, this can be increased several fold by elongated microcalcifications. The most dangerous situation is when a microinclusion appears in close proximity to a region where the PCS is already high. This stress will be substantially increased if the inclusion is elongated. In contrast, macrocalcifications at the cap shoulders are shown to actually increase plaque stability.

1 Introduction

Most acute coronary events and sudden coronary deaths have been associated with rupture of a thin fibrous cap overlying the necrotic core of thin-capped fibroatheroma (TCFA) followed by thrombosis (1-4). Despite major advances in treatment of coronary heart disease patients, a large number of victims of the disease, who are apparently healthy, die suddenly without prior symptoms. Available screening and diagnostic techniques are insufficient to identify the victims before the event occurs (5). The mechanism as to why some thin caps rupture and others do not is very likely the most important unanswered question in life threatening TCFAs.

Recently, we proposed a new hypothesis for the rupture of TCFA due to stress-induced interfacial debonding of minute (10 – 20 μm diameter) cellular-level microcalcifications in the cap proper (6). Such microcalcifications, which lie below the visibility of current in vivo imaging techniques, were detected for the first time using confocal microscopy and high resolution microcomputed tomography (micro-CT) imaging (6). The goal of this paper is to evaluate the impact of micro- and macrocalcifications on plaque biomechanical stability using 3D finite element (FE) analysis based on high resolution (7 μm) micro-CT imaging. In order to include the analysis of all types of coronary calcification, we developed a novel multi-level structural model of a human atherosclerotic lesion which consists of a macro-scale global model and two nested submodels, one at the level of the necrotic core and the other at the level of the microinclusions. The macro-

* Department of Biomedical Engineering, The City College of New York, CUNY NY

† Corresponding author. Department of Mechanical Engineering, The City College of New York, CUNY NY. Phone: (212)650-5202, Fax: (212)650-8013, E-mail: weinbaum@ccny.cuny.edu

scale model of the whole plaque includes large millimeter size calcifications at the bottom of the lipid pool and at its shoulders. The lowest level micro-scale model, which represents a segment of the fibrous cap, has a FE mesh refined enough to treat the detailed stress distribution around one or more microcalcifications in the cap proper. Both submodels contain approximately 1.5 M tetrahedral elements.

One of the most important factors contributing to plaque rupture is believed to be the peak circumferential stress (PSC) in the fibrous cap ...(7-14). Several of these computational analyses have demonstrated that thin fibrous caps and large lipid pools increase PCS in the cap dramatically. This observation agrees with pathological postmortem studies of ruptured plaques ...(3, 15-17). The majority of existing FE models of atherosclerotic lesions are based on 2D geometries of the lesion cross-sections obtained from histology ...(7, 9-11, 18). Although histology provides excellent resolution and clear definition of soft tissue components, it can't retain the true morphology of a lesion with coronary calcification because some degree of decalcification is usually required to allow sectioning. It is also difficult to avoid distortion in obtaining adjacent sections and, therefore, hard to reconstruct 3D images. Chau *et al.* (19) used optical coherence tomography (OCT) as a basis for their 2D finite element analysis and showed that OCT can provide a more realistic geometry than histology by avoiding structural artifacts common to histological processing.

Structural analysis based on intravascular ultrasound imaging (IVUS) of human iliac vessel segments performed before *in vitro* balloon angioplasty has been used to predict the locations of plaque fracture that usually accompanies angioplasty (8). Ohayon *et. al.* (20) performed a 2D FE analysis based on IVUS images of atherosclerotic coronary arteries recorded before and after balloon angioplasty to predict *in-vivo* plaque rupture locations. Recently, a 3D MRI based computational model of human atherosclerotic plaque with multi-component plaque structure and fluid-structure interaction was developed by Tang *et al.* (14). Although OCT, IVUS and MRI can provide 3D data for plaque structure, in all these imaging techniques large calcifications are not clearly delineated and calcifications < 50 – 100 microns are invisible or hard to distinguish. In order to circumvent these limitations and create a more accurate 3D geometry of a coronary lesion including cellular microcalcifications in the cap, we have developed in this study a high resolution micro-CT based computational technique. Although the approach can't be applied to *in-vivo* analysis of plaque stability, the insights gained from the *in-vitro* method are intended as an invaluable tool for exploring the basic mechanisms of plaque rupture. The fact that high resolution micro-CT scanning combined with topographic reconstruction algorithms can provide an accurate morphological and quantitative analysis of macroscopic atherosclerotic lesions was first demonstrated by Langheinrich *et al.* (21). In addition, Vengrenyuk *et al.* (6) demonstrated that micro-CT imaging could also be used for clear detection of cellular-level microscopic calcifications in the thin fibrous caps of vulnerable lesions. To our knowledge, the present study is the first attempt to use micro-CT imaging data sets to generate realistic plaque geometries and 3D finite element meshes for computational analysis of biomechanical plaque stability.

In our previous paper (6), the quantitative feasibility of our hypothesis for vulnerable plaque rupture due to the presence of cellular-level microcalcifications in the fibrous cap was evaluated using a model of a perfectly bonded spherical inclusion arbitrarily positioned in an elastic cap of uniform thickness under tension. First, we derived a local analytical solution of the 3D boundary value problem using linear elasticity. This solution predicted a nearly twofold increase in the local peak tensile stress around the embedded particle at the poles of the tensile axis. Then, we combined this local analytical solution for the stress concentration around the microcalcification with the histology based 2D finite element solution for circumferential stresses in a fibrous cap previously obtained by Finet *et al.* (11). Our results showed that inclusions located in an area of high circumferential stress (>300 kPa) in the cap can inten-

sify this stress to nearly 600 kPa, higher than the average rupture threshold, 545 kPa (7), when the cap thickness is < 65 μm, in close agreement with pathology observations (16, 17). Our original idealized model also provided a plausible explanation for the paradoxical observation that 40% of ruptures occurred in the center of the cap where FE calculations didn't predict maximum stresses (7, 22). In this paper, we develop a much more sophisticated multi-level FE model of these cellular-level microcalcifications in the cap proper and perform a 3D computational analysis using our detailed micro-CT reconstruction. This reconstruction includes the shape of the microcalcifications, their proximity to one another and their relationship to the cap thickness. A recent paper, which also attempts to evaluate the role of microcalcifications in plaque vulnerability, examines an idealized 3D geometry of an eccentric arterial stenosis with a single spherical microinclusion in the cap proper (23). This model, which is based on a fluid structure interaction numerical approach, does not attempt a detailed reconstruction of an actual plaque geometry, but has the advantage that it also provides the local wall shear stress distribution.

2 Methods

2.1 Micro-CT imaging

A 25 mm length proximal segment of the Left Circumflex human coronary artery (LCx) obtained at autopsy was scanned with the eXplore SP Pre-Clinical Specimen micro-CT acquisition and analysis system (GE Healthcare, Piscataway, NJ). For image acquisition, 720 consecutive x-ray projections were taken, obtaining 7-μm isotropic voxel resolution images. Mineral density was calibrated by using a phantom containing hydroxyapatite, air, and water. Initial reconstruction of the whole volume was carried out at 35-μm voxel resolution. Because of computational limitations, the initial volume was sectioned in consecutive volumes of interest consisting of the whole vessel cross section by about 3 mm in height, which were reconstructed at 7 μm resolution. Density-calibrated images were segmented by using the global threshold method built-in MicroView visualization and analysis software (GE Healthcare; Version 2.1.2). The presence of mineral, soft tissue, lipid, and air in the vessels was distinguished by the high sensitivity of the system to the different densities of each of these compartments. Mineralized tissue particles were investigated in each volume of interest, and isosurfaces of microcalcifications in the fibrous cap of the atherosclerotic lesion were rendered using the MicroView software.

2.2 3-D Reconstruction of Plaque Geometry and Tissue Property assignment

The 3-D micro-CT imaging data set obtained from the coronary segment was transferred to an image processing and segmentation software Mimics (Materialize). 3D plaque geometry and FE surface meshes were created by Mimics and exported to a commercial finite element package, ABAQUS 6.7.3, to build a volumetric tetrahedral mesh corresponding to the segment. The mesh was sent back to Mimics for property assignment based on the gray scale level attenuation of the original image data. In previous computational studies of atherosclerotic plaque two major material models were used, the linear elastic model (7, 8, 11) and the hyperelastic Mooney-Rivlin model ...(10, 13, 14, 19). In this paper, material mechanical properties were approximated by linearly elastic materials (Table 1 from (7)). To take into account the complex structure of the plaque constituents, we used a transverse isotropic material model, which assumes that the deformable medium has the same properties in the circumferential and axial direction. Lipid and calcifications were modeled as incompressible, isotropic materials with a Young's modulus of lipid equal to 1/100 of the circumferential Young's modulus of a normal artery and the Young's modulus of the calcification 10 times that of the non-calcified tissue (7). The baseline model of the real coronary lesion was modified using morphological operations in Mimics in order to study the effect of cap thickness on the PCS in the lesion.

2.3 Finite Element Analysis

The computational analysis was carried out with a commercial finite element package, ABAQUS (version 6.7.3). The major difficulty for the 3D image based mesh generation was the resolution required to evaluate the stresses around microcalcifications of only 10 – 20 μm diameter. The size of the finite elements required needed to be much smaller than 1 micron. This would result in an unrealistically high number of elements to model the entire coronary segment. Thus, we used a submodeling technique available in ABAQUS to study in detail a small area of interest in a global model, in our case, a region of high stress around calcified inclusions in the cap. First, a global model for the entire coronary segment without microcalcifications in the cap was created based on low resolution (35 μm) micro-CT image reconstruction using a relatively coarse mesh. The static global stresses were calculated for a mean physiological blood pressure of 110 mmHg (14.6 kPa) applied to the luminal inner surface of the vessel. Then, we created two submodels corresponding to 1) a 1.2 mm thick cross section of the artery and 2) a segment of the fibrous cap with microcalcifications in it. These hierarchical submodels based on the high resolution (7 μm) micro-CT reconstructions had a much more refined mesh and were driven by the global solution.

3 Results

In order to investigate the impact of calcifications on biomechanical plaque stability we scanned with micro-CT a human coronary lesion with a lipid core, large mm-size calcifications in the vessel wall and microcalcifications in the fibrous cap. Fig.1A shows the sagittal section of the segment, fig. 1B is a cross section of the same segment corresponding to the plane indicated by the arrow in Fig.1A. This cross section has two nearly spherical macrocalcifications, $\approx$ 300 μm in diameter, three microcalcifications ($\approx$ 10-20 μm in diameter, circled) in a thick fibrous cap ($\approx$ 300 μm). Numerous calcific deposits (arrows) can be observed at the bottom of the lipid pool. Fig. 1C shows the 3D vessel geometry reconstructed with

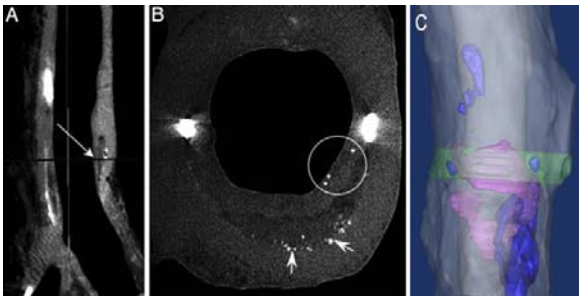

Figure 1: Micro-CT images (A, B) and reconstructed 3D geometry (C) of a coronary plaque with bulk calcifications (white in A and B, blue in C) and lipid core (dark areas in A and B, red in C). A small segment of the global model (green) containing fibrous cap with microcalcifications represents the first level submodel shown in detail in Fig.2A.

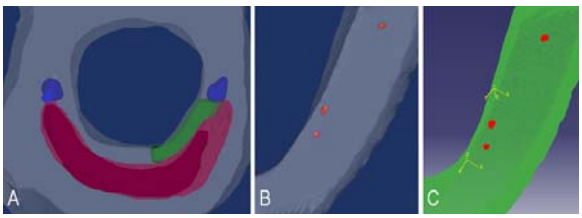

Figure 2: The hierarchy of Mimics/ABAQUS submodels. The first level submodel with macrocalcifications at the plaque shoulders (blue), lipid pool (red) and fibrous cap doesn't include microcalcifications in the cap (A). The submodel's cap fragment shown in green represents the second level submodel (B,C) which contains three microcalcifications.

Mimics.

We used the ABAQUS submodeling technique to focus on the fibrous cap with microcalcifications for detailed stress analysis. For each modeling level a mesh convergence study was performed in order to create a finite element mesh that balances accuracy and computing resources. We kept increasing the Mimics generated mesh density and reanalyzing the model until the difference between results from two consecutive meshes was negligible. The global model mesh corresponding to the whole vessel (1C) consisted of 2.5 million tetrahedral elements with the average length of

edges ≈80μm. Calculated stresses and displacements were used to drive the first level submodel shown in green in Fig. 1C. The submodel represents a 1.2 mm thick segment of the whole vessel where the area of maximum circumferential stress was observed. The submodel's morphological structure is shown in Fig. 2A. The lipid core (red), fibrous cap and macrocalcifications (blue) at plaque shoulders are included in the submodel consisting of 1.5 million elements (average length of edges ≈ 30μm). At the first level of submodeling microcalcifications in the fibrous cap were not considered due to the large size of the elements. Only the second level submodel (Fig.2B) which corresponds to a segment of the fibrous cap shown in green in Fig. 2A has a finite element mesh refined enough to include microcalcifications. The average edge of its 1.4 million elements was ≈ 0.3 μm (Fig. 2B).

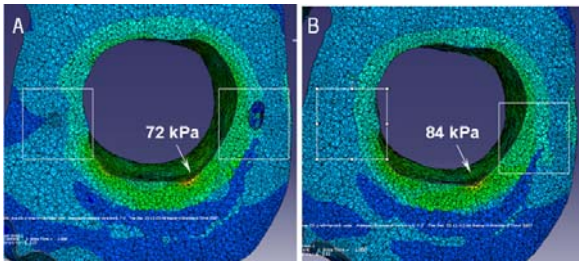

Figure 3: Circumferential stress distribution within the cross section. Maximum circumferential stress of 84 kPa without shoulder calcifications in 3B is reduced to 72 kPa in 3A in the presence of shoulder calcifications. Detailed stresses in the inserts are shown in Fig. 4 A and C.

First, we calculated the 3D stress distribution due to the mean physiological blood pressure of 110 mmHg in the entire segment without microcalcifications (Fig.1C). Analysis of the results revealed that the global maximum of circumferential stress was observed in the fibrous cap area where macrocalcifications at the plaque shoulders and microcalcifications in the cap are located (Fig.1B). Fig. 3A shows the stress distribution in the plaque cross section. The maximum circumferential stress is 72 kPa.

In order to analyze the effect of macrocalcifications at the plaque shoulders on the global stresses in the lesion, we created a model with two calcifications replaced by fibrotic tissue. All other morphological features and load conditions were the same. The results showed that the location of the maximum stress didn't change, but its magnitude increased to 84 kPa (Fig.3B). The observed stress reduction in the cap due to plaque calcification supports the idea that large calcifications have a stabilizing effect on the plaque.

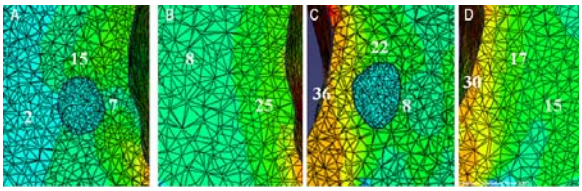

Figure 4: Local stress concentration around shoulder calcifications.

The model without macrocalcifications at the plaque shoulders in Fig. 3B allowed us to analyze the impact of the macrocalcific inclusions on the local stresses in the vessel wall by providing the background stresses. Figs. 4A,C show the detailed stress concentration around the macrocalcifications in the two inserts in Fig. 3A. Figs. 4B,D show stress distribution in the two inserts from Fig. 3B in the absence of the shoulder calcifications. Stress concentration can be observed around both calcifications in the direction of applied load at the poles of the inclusions (15 and 22 kPa in A and C compared to 8 and 17 kPa in B and D). The calcification in A also shows stress reduction at the equator from 25 kPa to 7 kPa, while the calcification in C doesn't have the area of reduced stress, the stress is actually increased from 30 to 36 kPa. In summary, the presence of two macrocalcifications at the plaque shoulders doesn't change maximum local stress significantly, but rather causes stress redistribution. We used the second level submodel to evaluate the stress concentration around microcalcifications in the fibrous cap proper. The results shown in Fig. 5 demonstrate that the PCS at the inclusions - cap interface reach 96.2, 54.9 and 37.8 kPa. Since the background circumferential stress in the cap without inclusions was 42.6 kPa, 28 kPa and 18 kPa,

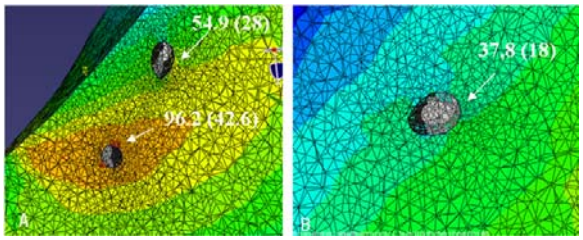

Figure 5: Stress concentration around microcalcifications in the thick fibrous cap of the original lesion circled in Fig. 1. Maximum local stress concentration (96.2 kPa) is higher than the global PCS in the same cap without microcalcifications.

stress concentration coefficients for the three calcifications are 2.25, 1.96 and 2.1 which is very close to the factor of two predicted by our analytical model of a spherical inclusion (6). Fig. 5A demonstrates that stress concentration around one of the inclusions located in a high stress area of 42.6 kPa reaches 96.2 kPa. This is higher than the global maximum stress of 72 kPa in the cap without microcalcifications shown in Fig. 3A. These results show that the inclusion of cellular-level microcalcifications resulted in a significant (33%) increase of the PCS in the thick-capped fibroatheroma and a doubling of the local stress. Another result of this analysis is that the location of the maximum stress has shifted from the lumen side of the cap to the interface between the inclusion and soft tissue.

The goal of our next numerical simulation was to investigate the effect of microcalcifications on the PCS as a function of cap thickness. We applied Mimics morphological operations to our baseline geometry of a thick-capped fibroatheroma to simulate the cap thinning process. A series of 3D models with cap thickness decreasing from the original value of 300 μm to 40 μm were created using fibrous cap erosion and lipid core dilation. As a result of fibrous cap thinning lipid core volume increased from 1.44 mm^3 corresponding to the original lesion shown in Fig. 1 to 5.8 mm^3 for the 40 μm cap model. For each of these models the global peak circumferential stress in the fibrous cap and the maximum local stress around microcalcifications were calculated and plotted as a function of cap thickness in Fig. 6, lines 1 and 2 respectively. The graph shows that the presence of microcalcifications in the fibrous cap results in an additional area of high circumferential stress in the cap. Both peak stresses increase exponentially as a result of reducing fibrous cap thickness. While our original thick-capped (300 μm) model predicted a global PCS of 72 kPa and a maximum local stress around calcifications of 96.2 kPa, the 40 μm thin-caped model predicted a PCS of 435 kPa and a maximum local stress around microcalcifications of 344 kPa. Although the global PCS in the thin-caped models (cap thickness < 80 μm) is higher than the local stress concentration around the microcalcifications, this local stress also reaches the rupture threshold of 300 kPa for cap thicknesses < 50 μm and, therefore, can increase the vulnerability of the lesion. In order to simulate the maximum destabilizing effect of microcalcifications, we also placed them in the area of the global PCS, and recalculated the maximum local stresses due to their presence. This result is plotted in Fig.6, line 3. Note that PCS is nearly doubled for all cap thicknesses, as previously predicted in (6) for a spherical micro-inclusion.

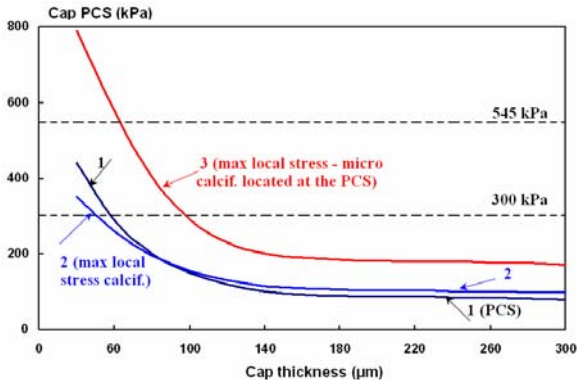

Figure 6: Global PCS in the fibrous cap (line 1) and maximum local stress around the original microcalcifications in Figs. 2B,C (line 2) in the "cap thinning" simulation. Line 3 corresponds to the maximum stresses around spherical microcalcifications located within the region of global PCS. Note PCS for curve 3 is approximately double that for curve 1.

The present 3D FEM also allowed us to estimate

the effect of calcification shape on the stability of fibrous cap atheroma. Lines 2 and 3 in Fig. 7 show how the global PCS in the cap would increase if an elliptical calcific inclusion with aspect ratio λ = b/a = 2 and 4, respectively, was located in the region of PCS with major axis b along the tensile axis. The stresses indicated by line 1 are the cap PCS with a spherical inclusion (λ = 1). Results of the calculations presented in Fig. 7 show significant increase in stress concentration with increase of the inclusion aspect ratio.

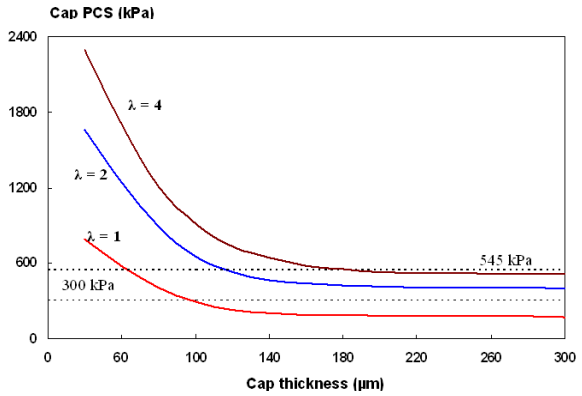

Figure 7: The effect of calcification shape at the cap PCS. Local maximum stress concentration around elliptical calcific inclusions located at the area of global PCS. Lines 1 – 3 correspond to the aspect ratios λ = b/a = 1, 2, 4. Note PCS for aspect ratio = 4 is nearly three times that for aspect ratio = 1.

Finally, the effect of microcalcification proximity on biomechanical plaque stability was evaluated by using confocal images of Alizarin Red S - stained microcalcifications in a fibrous cap of a human coronary lesion published in Vengrenyuk *et al.* (6). Fig. 8A shows the 3D confocal image reconstruction of these calcific inclusions, one the size of a single cell (10 μm) and the other an elongated calcification that is several times the diameter of the single-cell inclusion. We created an idealized 3D model of these inclusions based on the confocal image reconstruction and calculated the stress distribution around them when a uniform tension is applied in the direction of the long axis of the larger inclusion. Results of the calculations presented in Fig. 8B predict that the maximum stress between calcifications near the pole of the elongated inclusion can intensify the cap circumferential stress about 6 times. The high value of stress intensification can be explain by the fact that 1) the elongated inclusion's shape is close to an elliptical inclusion with a high aspect ratio, and 2) there is a superposition of local maximum stresses around inclusion poles due to their close proximity.

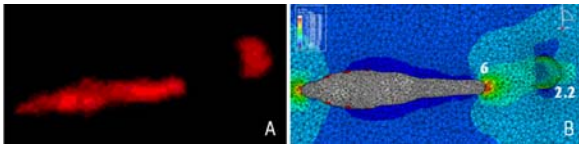

Figure 8: Stress concentration in a fibrous cap due to the presence of two adjacent calcifications stained with Alizarin Red S (A). An area of high circumferential stress is observed between the inclusions with a stress concentration of 6 at the pole of the elongated inclusion (B).

4 Discussion

In this paper, we have developed a new micro-CT based multi-scale FEM of atherosclerotic lesions and have applied the technique to evaluate the impact of calcifications of different size, shape and location on biomechanical plaque stability under a static load with a mean arterial pressure of 110 mmHg. Computational analysis of a thick-capped fibroatheroma predicted that the large calcification at the plaque shoulders and microscopic calcific inclusions in the fibrous cap have an opposite effect on the lesion stability. While the shoulder calcification have been shown to reduce the PCS in the cap by 16%, Fig.3, the presence of the micro-calcification in the cap increased the PCS by 33%, Figs. 5 and 6. This modest increase occurred because the micro-calicifications in Fig. 5 were not in a region where the background stress in the absence of micro inclusions was a maximum. A much larger PCS would be obtained if the micro-inclusion were located in region where the background stress was close to a region of PCS without the inclusion as shown by curve 3 in Fig. 6.

It is known that the size of the lipid core and fibrous cap thickness have the most significant effect on the stress background level within a TCFA. Fibrous cap thinning due to enzymatic degradation (3) may lead to increase of stresses and conversion of a stable plaque to a rupture prone or vulnerable lesion. We used Mimics morphological operations, namely, lipid pool dilation and fibrous cap erosion and created a series of fibroatheromas with cap thickness decreasing from 300 μm to 40 μm to model the "cap thinning" process in (3). The results showed the presence of an additional area of high circumferential stress in the cap due to the local stress concentration around microcalcifications in all generated models for the microinclusions shown in Figs. 2B,C. Although this maximum local stress around micro-inclusions was lower than the global PCS for caps < 80 μm thickness, see Fig. 6, its value for a cap thickness of 40 μm was 344 kPa, more than the rupture threshold of 300 kPa. However, the thickness of the fibrous cap and the size of the lipid core are not sufficient to predict cap stability. The results in Fig. 6 indicate that the most significant impact on plaque stability occurs when microcalcifications are located in close proximity to a region of PCS.

To our knowledge, this study represents the first attempt to use high resolution micro-CT imaging for an *in-vitro* 3D FE analysis of an atherosclerotic lesion. Most existing FEMs of atherosclerotic lesions are based on 2D geometries of the lesion cross-section obtained from histology, OCT, IVUS or MRI (7, 9-11, 13, 14, 18). Currently, histology is considered to be the “gold standard” for determining plaque geometry and composition. Although it provides excellent resolution and clear definition of plaque morphology, histological processing and sectioning introduces artifacts, especially in plaques with calcifications present. In OCT, IVUS and MRI large calcifications are not clearly delineated and microcalcifications < 50-100 μm are invisible except for OCT. We used high resolution (7 μm) micro-CT imaging data to generate realistic 3D geometries of a coronary lesion with several large mm size calcifications and microcalcifications (10 – 20 μm) in the fibrous cap and combined this with a multi-level submodeling technique in ABAQUS. Our simulations strongly suggest that this approach is the best approach to analyze the role of coronary calcium in plaque stability *in-vitro*. In addition, it can be also used for analyzing the potential impact of coronary calcification on the outcome of balloon angioplasty, stenting procedures, coronary artery bypass grafting and other surgical procedures.

The calculated stress concentration coefficients around macro- and microcalcifications in the lesion are very close to the values predicted by our analytical model of an idealized spherical inclusion in an elastic cap of uniform thickness under tension (6). Both calcifications approximately doubled the background stress due to the fact that the inclusion shape is close to spherical and they are located far from each other. In addition, our results in Figs. 7 and 8 indicate that microcalcification shape can have a dramatic effect on plaque stability. The presence of an elliptical calcification with an aspect ratio, $\lambda = 4$, in a fibrous cap can intensify the PCS in the cap by a factor of three beyond that for a spherical inclusion. The most significant, a 6 - fold increase in stress, was predicted in Fig. 8 for an elongated inclusion in close proximity to a spherical one. The results suggest that microcalcification shape and positioning have a profound effect on plaque stability. The concept of local stress induced interfacial debonding is discussed more fully in (6). Basically, in any liquid filled material if a vacuum is created at a tiny crevice along a solid interface, a small cavitation bubble will form which expands greatly with small further increases in interfacial tension. This phenomenon is readily observed for small solid inclusion in polymeric materials.

There is an extensive literature based on *in vivo* IVUS, OCT and MRI imaging that attempts to correlate plaque burden with the prediction of future coronary events. This literature, which is inconclusive, is briefly summarized below since it pervades current thinking. It is very difficult to critically analyze this literature unless one is able to identify a mechanism for cap instability. The calculations in this paper and the hypothesis pro-

posed by Vengrenyuk *et al.* (6) propose such a mechanism. Unfortunately, the entire current literature, which is based on *in vivo* imaging, fails to capture the cellular level microcalcifications in the cap proper that are analyzed in the present paper and in Vengrenyuk *et al.* (6). These cellular level inclusions fall below the visibility of these *in vivo* imaging techniques and their statistic frequency in TCFA has not yet been established. In addition, the term speckled or diffuse calcification used in the literature can also apply to calcified macrophages and smooth muscle cells that reside in the lipid pool and, as such, can be considered floating debris. These small calcifications have no effect on plaque stability since they are imbedded in tissue with small or no tensile stresses (these tensile stresses vanish in the lipid pool).

With the foregoing caveats we briefly analyze some of the better known papers that try to correlate calcified plaque burden with plaque stability. In one series of studies of sudden coronary death cases, over 50% of nonruptured TCFA showed a lack of macrocalcification or only speckled calcification on post-mortem radiographs of coronary arteries (24). In contrast, 65% of ruptured lesions demonstrated speckled calcification, with the reminder showing fragmented or diffuse calcification. Furthermore, the mean calcification score was significantly higher in ruptured than in nonruptured vulnerable plaques. The authors concluded that these data demonstrate the lack of specificity of calcium patterns in unstable coronary plaques, but suggest that mildly to moderately calcified segments are the most likely to rupture. IVUS studies, on the other hand, have led to an opposing view of the importance of calcification. Rasheed *et al.* (25) showed that unstable clinical symptoms are associated with quantitatively less calcium. Similarly, Beckman *et al.* (26) observed that culprit lesions in patients with stable angina pectoris (SAP) were more extensively calcified than those in unstable angina pectoris patients (UAP) and that patients who have had an acute myocardial infarction (AMI) had the least calcified culprit lesions. Subsequently, Ehara *et al.* (27) recognized that there was a significant difference in the pattern of coronary calcifications between patients with AMI, UAP, and SAP. They observed that small calcium deposits which subtended an arc of <90°(e.g. the macrocalcifications at the shoulders seen in Fig.1) from the center of the vessel and were described as "spotty" calcification, were significantly more frequent in the culprit lesions of AMI as opposed to SAP patients. The culprit lesions of AMI patients were mostly characterized by small macroscopic calcium deposits. These authors suggest that it is not the identification of calcium per se that is important, but rather the size, extent and location of the deposits. This conclusion is supported by an IVUS analysis by Fujii *et al.* (28), who showed that ruptured plaques had quantitatively less calcium, especially superficial calcification, but a larger number of small calcium deposits, especially deep calcium deposits. Spotty calcification was also associated with the culprit lesions in acute coronary syndromes studied noninvasively by multislice computed tomography (29). In contrast to the clinical observations that coronary artery calcification is associated with worse prognosis, several recent computational studies (10, 14, 30) demonstrated that macrocalcifications do not affect the lesion stability significantly. Histology based 2D finite Element Analysis in Huang et. al. (10) showed that arterial calcifications are actually stabilizing due to the fact that peak circumferential stresses are reduced when these calcifications are present. Our present results also support the stabilizing role of macrocalcifications, even when they occur in regions of large curvature, such as the cap shoulder.

In conclusion, we have attempted to define a new paradigm for plaque stability, namely local stress concentrations surrounding minute calcifications at the cellular level in the cap proper. Currently, these micro inclusions are most easily seen *in vitro* by micro-CT. It is clear from the present model calculations that cellular level calcifications by themselves are not dangerous unless they lie in a region of high background stress. This high level of background stress only occurs in caps whose thickness is $<$ approximately 80 μm. Whereas a spherical microcalcification will increase PCS by a factor of two this can be in-

creased several fold by elongated microcalcifications of the type depicted in Fig. 8. Even if a microcalcification does appear in a thin cap, if it is spherical in shape there is a good chance that the maximum stress surrounding the inclusion may not exceed the rupture threshold of 300 kPa defined by Cheng et al. (7), see Fig. 6. The most dangerous situation is when a microinclusion appears in close proximity to a region where the PCS is already high. Curve 3 in Fig. 6 shows that a spherical inclusion will intensify the local stress to 545 kPa, the average stress for rupture, in a region of PCS when the cap thickness is < 65 μm in close agreement with the observation of Virmani *et al.* (17). This stress will be substantially increased if the inclusion is elongated.

Acknowledgement: We would like to thank Dr. R. Virmani for helping us to uncover the first evidence for the existence of microcalcifications in a cap proper, to our collaborators S. Einav, J. Fallon and G. Randolph for insightful discussion of various parts of this manuscript, and Dr. M. B. Schaffler for his generous access in the micro-CT facility at the Department of Orthopaedics at Mount Sinai School of Medicine.

References

1. Burke, A. P., Farb A., Malcom G. T., Liang Y., Smialek J. E., & Virmani R. (1999) JAMA 281, 921-926.

2. Burke, A. P., Farb A., Malcom G. T., Liang Y. H., Smialek J., & Virmani R. (1997) N Engl J Med 336, 1276-1282.

3. Virmani, R., Kolodgie F. D., Burke A. P., Farb A., & Schwartz S. M. (2000) Arterioscler Thromb Vasc Biol 20, 1262-1275.

4. Libby, P., Ridker P. M., & Maseri A. (2002) Circulation 105, 1135-1143.

5. Naghavi, M., Libby P., Falk E., Casscells S. W., Litovsky S., Rumberger J., Badimon J. J., Stefanadis C., Moreno P., Pasterkamp G., *et al.* (2003) Circulation 108, 1664-1672.

6. Vengrenyuk, Y., Carlier S., Xanthos S., Cardoso L., Ganatos P., Virmani R., Einav S., Gilchrist L., & Weinbaum S. (2006) Proc Natl Acad Sci U S A 103, 14678-14683.

7. Cheng, G. C., Loree H. M., Kamm R. D., Fishbein M. C., & Lee R. T. (1993) Circulation 87, 1179-1187.

8. Lee, R. T., Loree H. M., Cheng G. C., Lieberman E. H., Jaramillo N., & Schoen F. J. (1993) J Am Coll Cardiol 21, 777-782.

9. Loree, H. M., Kamm R. D., Stringfellow R. G., & Lee R. T. (1992) Circ Res 71, 850-858.

10. Huang, H., Virmani R., Younis H., Burke A. P., Kamm R. D., & Lee R. T. (2001) Circulation 103, 1051-1056.

11. Finet, G., Ohayon J., & Rioufol G. (2004) Coron Artery Dis 15, 13-20.

12. Tang, D., Yang C., Kobayashi S., & Ku D. N. (2004) J Biomech Eng 126, 363-370.

13. Tang, D., Yang C., Zheng J., Woodard P. K., Saffitz J. E., Petruccelli J. D., Sicard G. A., & Yuan C. (2005) Ann Biomed Eng 33, 1789-1801.

14. Tang, D., Yang C., Zheng J., Woodard P. K., Saffitz J. E., Sicard G. A., Pilgram T. K., & Yuan C. (2005) J Biomech Eng 127, 1185-1194.

15. Cheruvu, P. K., Finn A. V., Gardner C., Caplan J., Goldstein J., Stone G. W., Virmani R., & Muller J. E. (2007) J Am Coll Cardiol 50, 940-949.

16. Kolodgie, F. D., Burke A. P., Farb A., Gold H. K., Yuan J., Narula J., Finn A. V., & Virmani R. (2001) Curr Opin Cardiol 16, 285-292.

17. Virmani, R., Burke A. P., Kolodgie F. D., & Farb A. (2003) J Interv Cardiol 16, 267-272.

18. Richardson, P. D., Davies M. J., & Born G. V. (1989) Lancet 2, 941-944.

19. Chau, A. H., Chan R. C., Shishkov M., MacNeill B., Iftimia N., Tearney G. J., Kamm R. D., Bouma B. E., & Kaazempur-Mofrad M. R. (2004) Ann Biomed Eng 32, 1494-1503.

20. Ohayon, J., Teppaz P., Finet G., & Rioufol G. (2001) Coron Artery Dis 12, 655-663.

21. Langheinrich, A. C., Bohle R. M., Greschus S., Hackstein N., Walker G., von Gerlach S., Rau W. S., & Holschermann H. (2004) Radiology 231, 675-681.

22. Maehara, A., Mintz G. S., Bui A. B., Walter O. R., Castagna M. T., Canos D., Pichard A. D., Satler L. F., Waksman R., Suddath W. O., *et al.* (2002) J Am Coll Cardiol 40, 904-910.

23. Bluestein, D., Alemu Y., Avrahami I., Gharib M., Dumont K., Ricotta J., & Einav S. (2008) Journal of Biomechanics (in press).

24. Burke, A. P., Weber D. K., Kolodgie F. D., Farb A., Taylor A. J., & Virmani R. (2001) Herz 26, 239-244.

25. Rasheed, Q., Nair R., Sheehan H., & Hodgson J. M. (1994) Am J Cardiol 73, 753-758.

26. Beckman, J. A., Ganz J., Creager M. A., Ganz P., & Kinlay S. (2001) Arterioscler Thromb Vasc Biol 21, 1618-1622.

27. Ehara, S., Kobayashi Y., Yoshiyama M., Shimada K., Shimada Y., Fukuda D., Nakamura Y., Yamashita H., Yamagishi H., Takeuchi K., *et al.* (2004) Circulation 110, 3424-3429.

28. Fujii, K., Carlier S. G., Mintz G. S., Wijns W., Colombo A., Bose D., Erbel R., de Ribamar Costa J., Jr., Kimura M., Sano K., *et al.* (2005) Am J Cardiol 96, 1476-1483.

29. Motoyama, S., Kondo T., Sarai M., Sugiura A., Harigaya H., Sato T., Inoue K., Okumura M., Ishii J., Anno H., *et al.* (2007) J Am Coll Cardiol 50, 319-326.

30. Imoto, K., Hiro T., Fujii T., Murashige A., Fukumoto Y., Hashimoto G., Okamura T., Yamada J., Mori K., & Matsuzaki M. (2005) J Am Coll Cardiol 46, 1507-1515.